Electronic Supplementary Information

In-situ self-doped biomass-derived porous carbon as excellent oxygen reduction electrocatalyst for fuel cell and metal-air battery

Menggeng Hao,[ab] Rongmin Dun,[b] Yumiao Su,[a] Lei He,[c] Fandi Ning,[c] Xiaochun Zhou*[c] and Wenmu Li*[a]

[a] Fujian Institute of Research on the Structure of Matter, Chinese Academy of Sciences, Fuzhou 350002, P. R. China

[b] University of Chinese Academy of Sciences, Beijing 100049, China

[c] Suzhou Institute of Nano-Tech and Nano-Bionics (SINANO), Chinese Academy of Sciences, Suzhou, 215123, China

E-mail: liwm@fjirsm.ac.cn ; xczhou2013@sinano.ac.cn

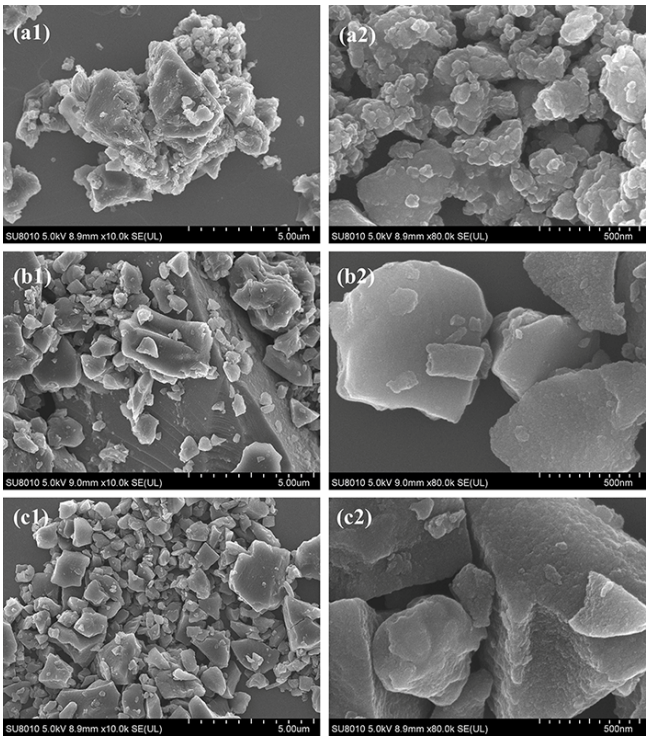

Fig. S1 SEM images of as-prepared catalysts at various temperatures: (a1-a2) RN350-1000; (b1-b2) RN350-Z(1-2)-700; (c1-c2) RN350-Z(1-2)-800.

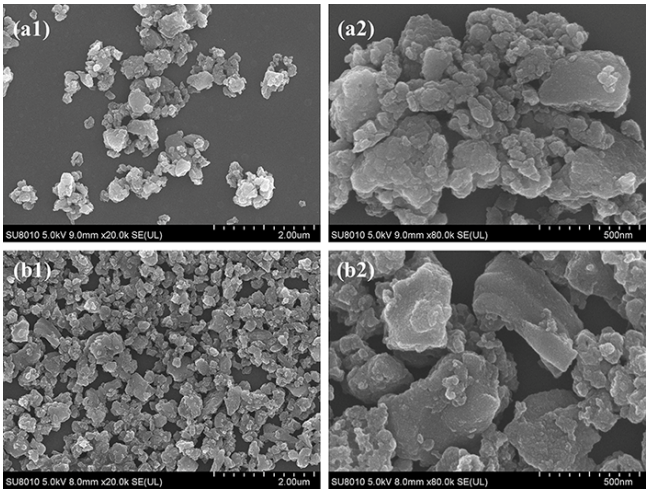

Fig. S2 SEM images of (a1-a2) RN350-Z(1-2)-900; (b1-b2) RN350-Z(1-2)-1000.

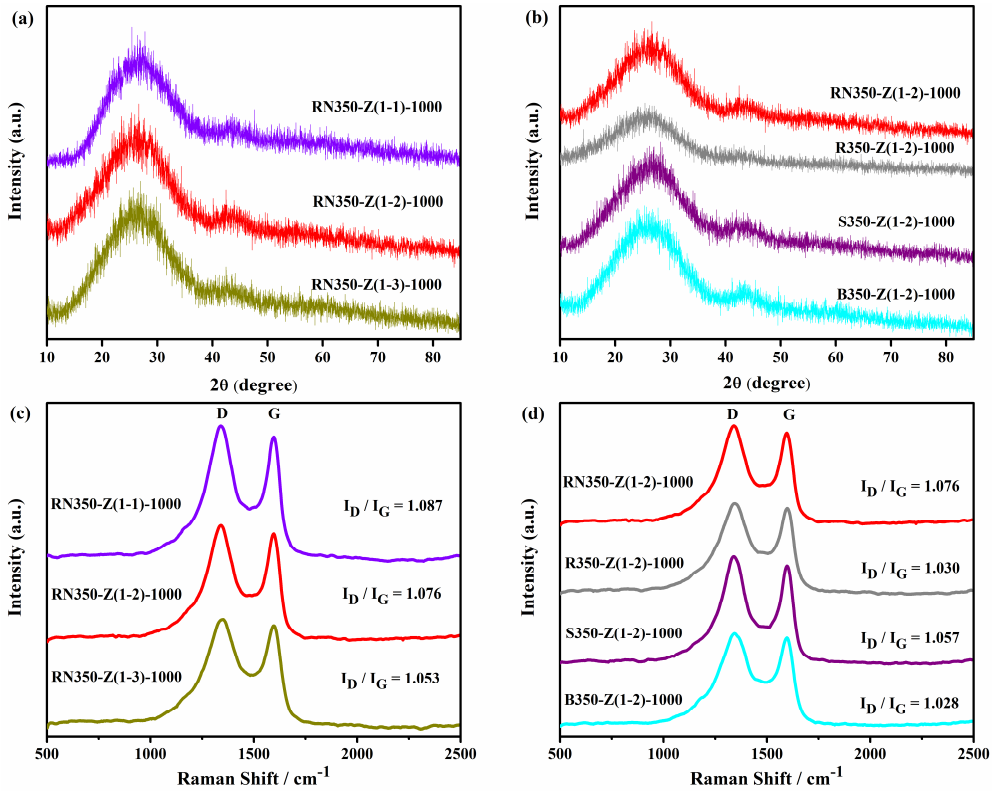

Fig. S3 (a) XRD pattern of RN350-Z(1-x)-1000 (x = 1, 2, 3). (b) XRD pattern of RN350-Z(1-2)-1000, R350-Z(1-2)-1000, S350-Z(1-2)-1000, and B350-Z(1-2)-1000. (c) Raman spectra of RN350-Z(1-x)-1000 with the corresponding I_D / I_G values. (d) Raman spectra of RN350-Z(1-2)-1000, R350-Z(1-2)-1000, S350-Z(1-2)-1000, and B350-Z(1-2)-1000 with the corresponding I_D / I_G values.

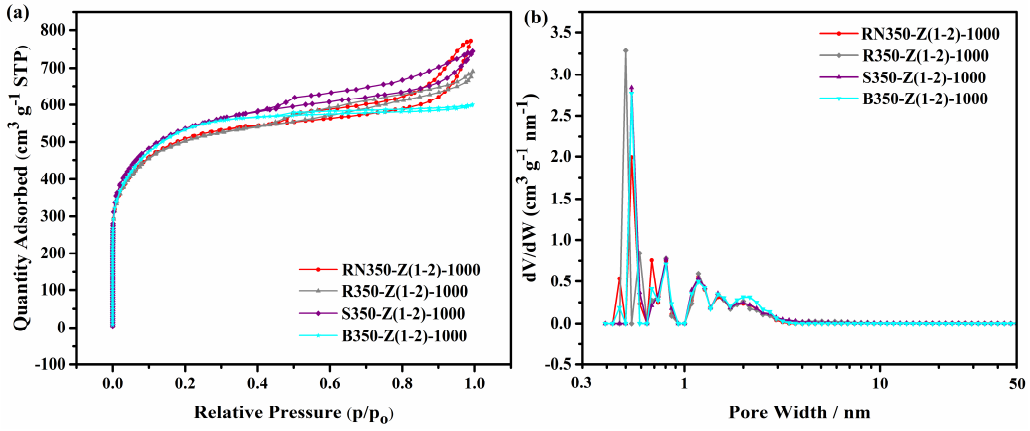

Fig. S4 (a) N_2 adsorption-desorption isotherms of RN350-Z(1-2)-1000, R350-Z(1-2)-1000, S350-Z(1-2)-1000, and B350-Z(1-2)-1000. (b) The corresponding pore size distributions.

Table S1. Textural properties of RN350-1000, RN350-Z(1-2)-T (T = 700, 800, 900, and 1000 °C).

Sample	S^{a}_{BET} (m^2/g)	S^{b}_{micro} (m^2/g)	S_{meso} (m^2/g)	V^{c}_{total} (cm^3/g)	V^{d}_{micro} (cm^3/g)	V_{meso} (cm^3/g)	Pore size [e] (nm)	
							Micro[f] (nm)	D_{av}[g] (nm)
RN350-1000	**440.13**	**192.01**	**248.12**	**0.3302**	**0.0823**	**0.2479**	**0.5538**	**3.00**
RN350-Z(1-2)-700	**1550.31**	**1106.43**	**443.88**	**0.7076**	**0.4558**	**0.2518**	**0.6016**	**1.83**
RN350-Z(1-2)-800	**1542.13**	**1010.23**	**531.90**	**0.7171**	**0.4246**	**0.2925**	**0.6012**	**1.86**
RN350-Z(1-2)-900	**1537.97**	**696.34**	**841.63**	**0.9402**	**0.2940**	**0.6462**	**0.6191**	**2.45**
RN350-Z(1-2)-1000	**1835.08**	**886.02**	**949.06**	**1.1942**	**0.3629**	**0.8313**	**0.6136**	**2.60**

[a] Surface area determined by the BET method.

[b] Micropore surface area determined by t-Plot micropore area.

[c] Total pore volume calculated by the DFT method.

[d] Micropore volume determined by t-Plot micropore volume.

[e] the pore distribution curves determined by the DFT method.

[f] Micropore width determined by the HK method.

[g] Average pore width determined by adsorption average pore width (4V/A by BET).

Table S2. Textural properties of RN350-Z(1-2)-1000, R350-Z(1-2)-1000, S350-Z(1-2)-1000, and B350-Z(1-2)-1000.

Sample	S_{BET} (m^2/g)	S_{micro} (m^2/g)	S_{meso} (m^2/g)	V_{total} (cm^3/g)	V_{micro} (cm^3/g)	V_{meso} (cm^3/g)	Pore size (nm)	
							Micro (nm)	D_{av} (nm)
RN350-Z(1-2)-1000	**1835.08**	**886.02**	**949.06**	**1.1942**	**0.3629**	**0.8313**	**0.6136**	**2.60**
R350-Z(1-2)-1000	**1794.18**	**887.07**	**907.11**	**1.0695**	**0.3723**	**0.6972**	**0.6101**	**2.38**
S350-Z(1-2)-1000	**1946.26**	**907.94**	**1038.32**	**1.1512**	**0.3680**	**0.7832**	**0.6167**	**2.37**
B350-Z(1-2)-1000	**1901.23**	**749.68**	**1151.55**	**0.9276**	**0.3109**	**0.6167**	**0.6149**	**1.95**

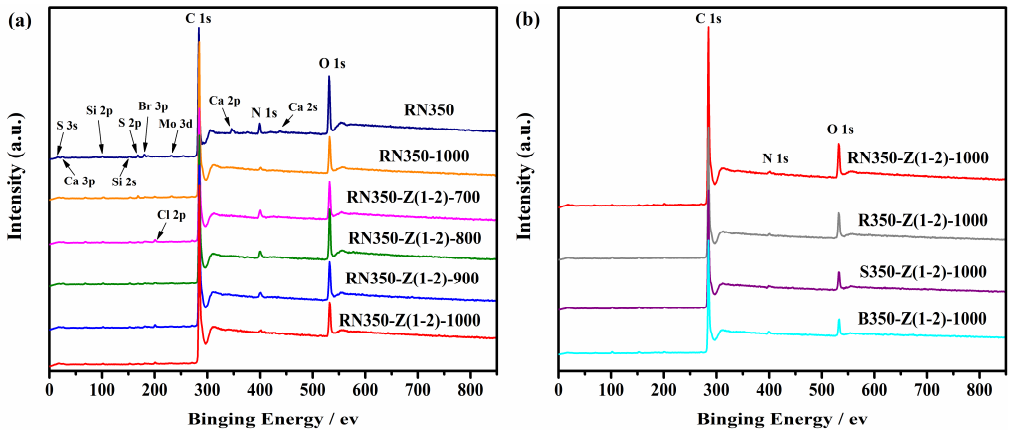

Fig. S5 (a) The full XPS spectra of RN350, RN350-1000, and RN350-Z(1-2)-T (T = 700, 800, 900, and 1000 °C). (b) The full XPS spectra of RN350-Z(1-2)-1000, R350-Z(1-2)-1000, S350-Z(1-2)-1000, and B350-Z(1-2)-1000.

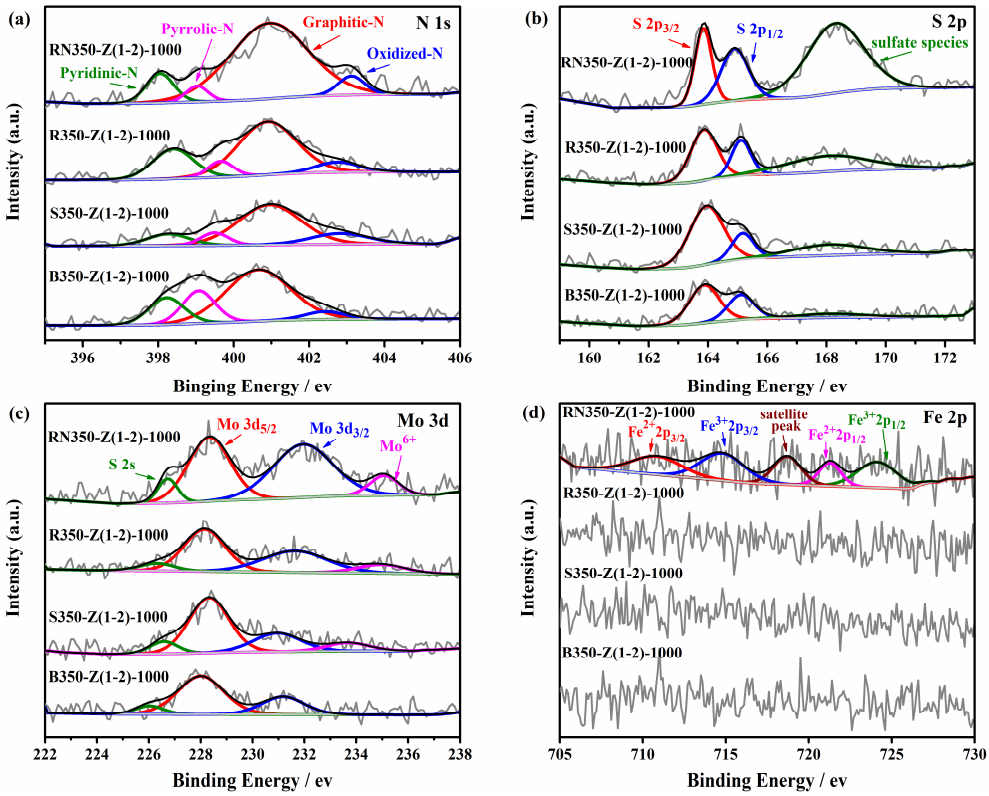

Fig. S6 (a) High-resolution N 1s spectra of RN350-Z(1-2)-1000, R350-Z(1-2)-1000, S350-Z(1-2)-1000, and B350-Z(1-2)-1000. (b) High-resolution S 2s spectra. (c) High-resolution Mo 3d spectra. (d) High-resolution Fe 2p spectra.

Table S3. Elemental compositions of RN350, RN350-1000, RN350-Z(1-2)-T (T = 700, 800, 900, and 1000 ℃), RN350-HF and RN350-HF-Z(1-2)-1000 calculated by XPS dates.

Sample	C (at %)	N (at %)	O (at %)	S (at %)	Mo (at %)	Fe (at %)	N-1 % (at %)	N-2 % (at %)	N-3 % (at %)	N-4 % (at %)
RN350	**78.45**	**4.51**	**16.12**	**0.81**	**0.11**	*	-	-	-	-
RN350-1000	**87.21**	**1.50**	**10.28**	**0.90**	**0.11**	*	**15.22 (0.229)**	**7.76 (0.116)**	**71.53 (1.073)**	**5.49 (0.082)**
RN350-Z(1-2)-700	**84.07**	**4.50**	**11.09**	**0.30**	**0.04**	*	**22.22 (1.000)**	**7.92 (0.356)**	**66.03 (2.972)**	**3.83 (0.172)**
RN350-Z(1-2)-800	**82.28**	**3.64**	**13.73**	**0.31**	**0.04**	*	**23.71 (0.863)**	**10.45 (0.380)**	**59.92 (2.181)**	**5.92 (0.216)**
RN350-Z(1-2)-900	**86.20**	**2.80**	**10.49**	**0.45**	**0.06**	*	**17.32 (0.485)**	**9.86 (0.276)**	**66.51 (1.862)**	**6.31 (0.177)**
RN350-Z(1-2)-1000	**88.94**	**1.45**	**9.20**	**0.36**	**0.05**	*	**10.69 (0.155)**	**4.65 (0.067)**	**77.99 (1.131)**	**6.67 (0.097)**
RN350-HF	**81.42**	**5.28**	**13.12**	**0.16**	**0.02**	*	-	-	-	-
RN350-HF-Z(1-2)-1000	**88.81**	**1.90**	**8.86**	**0.39**	**0.05**	*	**19.47 (0.370)**	**4.71 (0.089)**	**68.68 (1.305)**	**7.15 (0.136)**

N-1: Pyridinic-N; N-2: Pyrrolic-N; N-3: Graphitic-N; N-4: Oxidized-N.

***** Due to the content of Fe element is very small, the peak intensity of all high-resolution Fe 2p spectra are slight, which calculated by integrated area has a great error, therefore, the content of Fe element that calculated by XPS is negligible.

Table S4. Elemental compositions of RN350-Z(1-2)-1000, R350-Z(1-2)-1000, S350-Z(1-2)-1000, and B350-Z(1-2)-1000 calculated by XPS dates.

Sample	C (at %)	N (at %)	O (at %)	S (at %)	Mo (at %)	Fe (at %)	N-1 % (at %)	N-2 % (at %)	N-3 % (at %)	N-4 % (at %)
RN350-Z(1-2)-1000	**88.94**	**1.45**	**9.20**	**0.36**	**0.05**	*	**10.69 (0.155)**	**4.65 (0.067)**	**77.99 (1.131)**	**6.67 (0.097)**
R350-Z(1-2)-1000	**89.21**	**1.46**	**9.06**	**0.24**	**0.04**	*	**23.63 (0.345)**	**8.03 (0.117)**	**59.70 (0.872)**	**8.65 (0.126)**
S350-Z(1-2)-1000	**90.80**	**1.28**	**7.57**	**0.30**	**0.05**	*	**12.40 (0.159)**	**8.85 (0.113)**	**63.01 (0.807)**	**15.74 (0.201)**
B350-Z(1-2)-1000	**91.23**	**1.80**	**6.75**	**0.19**	**0.04**	*	**16.92 (0.305)**	**18.89 (0.340)**	**58.57 (1.054)**	**5.61 (0.101)**

Table S5. The content of C, N, H, and S for as-prepared samples were analyzed by elemental analysis (EA) measurement and the content of Mo and Fe were analyzed by inductive coupled plasma emission spectrometer (ICP) measurement.

	EA mass ratio (%)				ICP mass ratio (%)	
Sample	**C**	**N**	**H**	**S**	**Mo**	**Fe**
RN350	**63.60 / 63.65**	**5.13 / 5.12**	**4.37 / 4.35**	**0.76 / 0.54**	**0.0067**	**0.034**
RN350-1000	**76.44 / 76.90**	**1.26 / 1.28**	**1.42 / 1.48**	**<0.3**	**0.0010**	**0.017**
RN350-Z(1-2)-700	**68.95 / 69.11**	**4.82 / 4.81**	**3.08 / 3.07**	**0.40 / 0.39**	**0.0013**	**0.038**
RN350-Z(1-2)-800	**72.72 / 72.50**	**4.68 / 4.66**	**2.85 / 2.53**	**0.47 / 0.46**	**0.0017**	**0.0301**
RN350-Z(1-2)-900	**74.54 / 74.71**	**2.63 / 2.68**	**2.98 / 3.02**	**0.54 / 0.52**	**0.056**	**0.101**
RN350-Z(1-2)-1000	**63.37 / 64.83**	**1.25 / 1.27**	**2.30 / 2.35**	**0.37 / 0.40**	**0.031**	**0.106**
RN350-HF-Z(1-2)-1000	**62.58 / 62.86**	**1.51 / 1.59**	**2.31 / 2.04**	**0.60 / 0.55**	**0.0011**	**0.02**

Table S6. The content of C, N, H, and S were analyzed by elemental analysis (EA) measurement, and the content of Mo and Fe were analyzed by inductive coupled plasma emission spectrometer (ICP) measurement.

	EA mass ratio (%)				ICP mass ratio (%)	
Sample	**C**	**N**	**H**	**S**	**Mo**	**Fe**
RN350-Z(1-2)-1000	**63.37/ 64.83**	**1.25 / 1.27**	**2.30 / 2.35**	**0.37 / 0.40**	**0.031**	**0.106**
R350-Z(1-2)-1000	**81.66 / 81.58**	**1.38 / 1.35**	**3.10 / 3.24**	**0.32 / 0.32**	**0.0225**	**0.0401**
S350-Z(1-2)-1000	**84.34 / 84.48**	**0.90 / 0.92**	**2.85 / 2.76**	**0.41 / 0.42**	**0.0058**	**0.0248**
B350-Z(1-2)-1000	**76.52 / 76.39**	**1.54 / 1.50**	**1.27 / 1.14**	**0.45 / 0.49**	**0.0114**	**0.042**

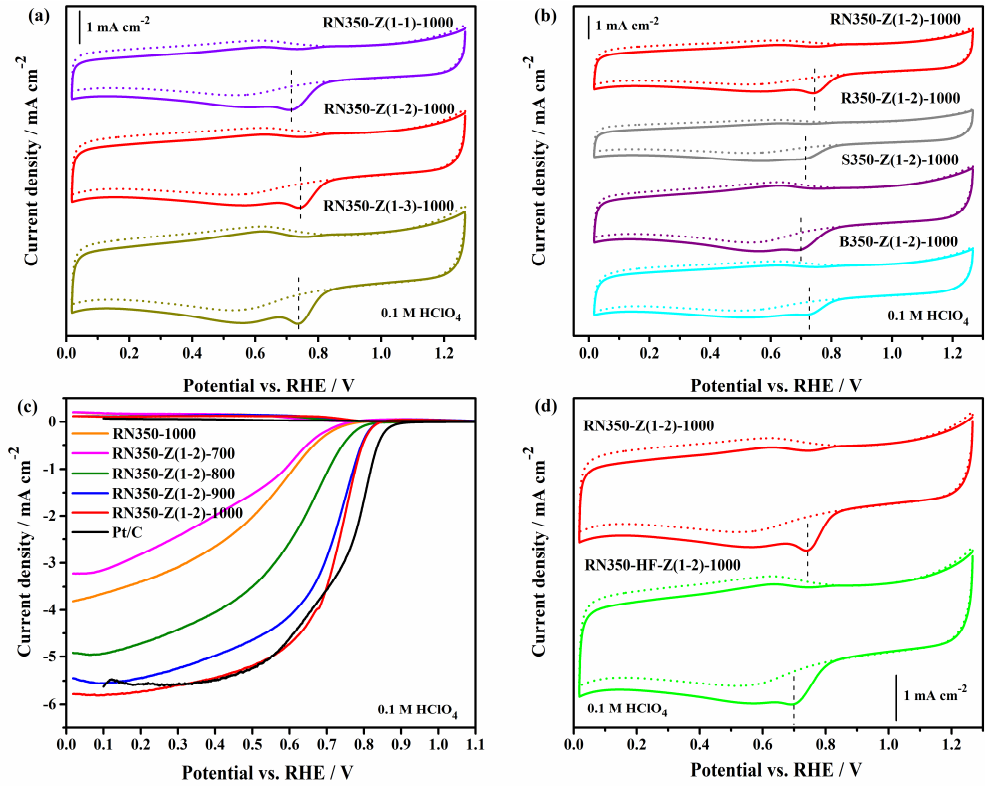

Fig. S7 (a) CV curves of RN350-Z(1-x)-1000 (x = 1, 2, 3) in O_2 or N_2-saturated 0.1 M $HClO_4$ solution at a scan rate of 10 mV s^{-1}. (b) CV curves of RN350-Z(1-2)-1000, R350-Z(1-2)-1000, S350-Z(1-2)-1000, and B350-Z(1-2)-1000 in 0.1 M $HClO_4$ solution. (c) Rotating ring disk electrode (RRDE) curves of as-prepared catalysts and Pt/C in O_2-saturated 0.1 M $HClO_4$ solution at a rate of 10 mV s^{-1} and a rotating rate of 1600 rpm. (d) CV curves of RN350-Z(1-2)-1000 and RN350-HF-Z(1-2)-1000 in O_2 or N_2-saturated 0.1 M $HClO_4$ solution.

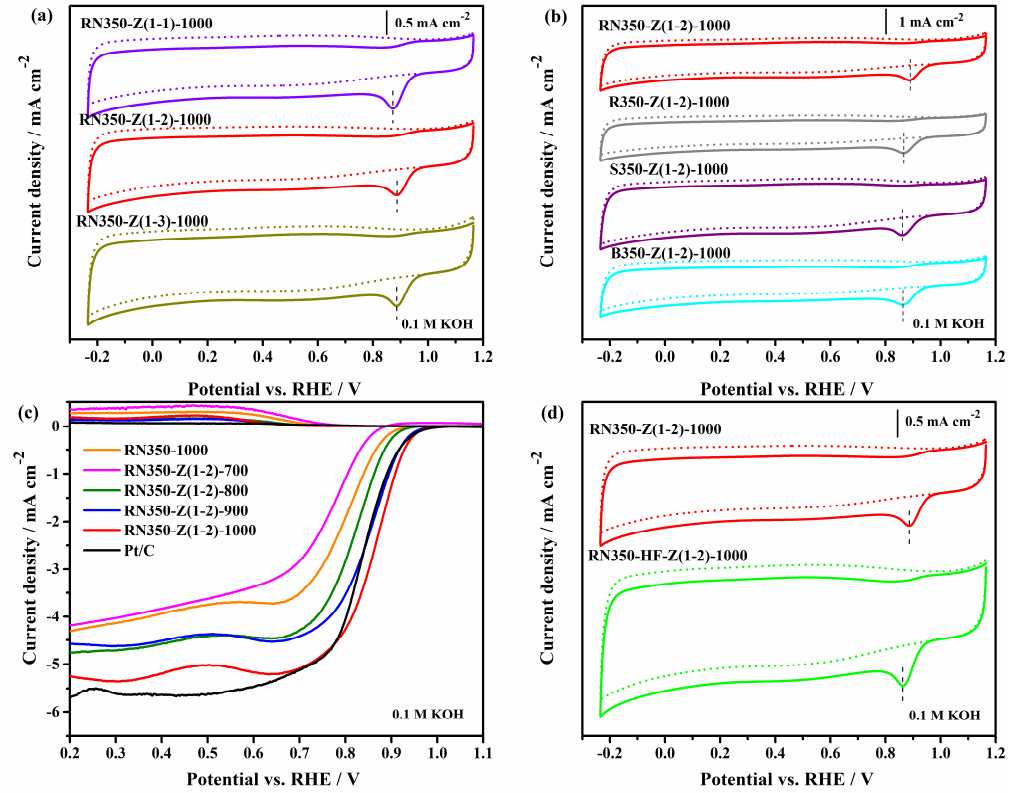

Fig. S8 (a) CV curves of RN350-Z(1-x)-1000 (x = 1, 2, 3) in O_2 or N_2-saturated 0.1 M KOH solution at a scan rate of 10 mV s^{-1}. (b) CV curves of RN350-Z(1-2)-1000, R350-Z(1-2)-1000, S350-Z(1-2)-1000, and B350-Z(1-2)-1000 in 0.1 M KOH solution. (c) Rotating ring disk electrode (RRDE) curves of as-prepared catalysts and Pt/C in O_2-saturated 0.1 M KOH solution at a rate of 10 mV s^{-1} and a rotating rate of 1600 rpm. (d) CV curves of RN350-Z(1-2)-1000 and RN350-HF-Z(1-2)-1000 in O_2 or N_2-saturated 0.1 M KOH solution.

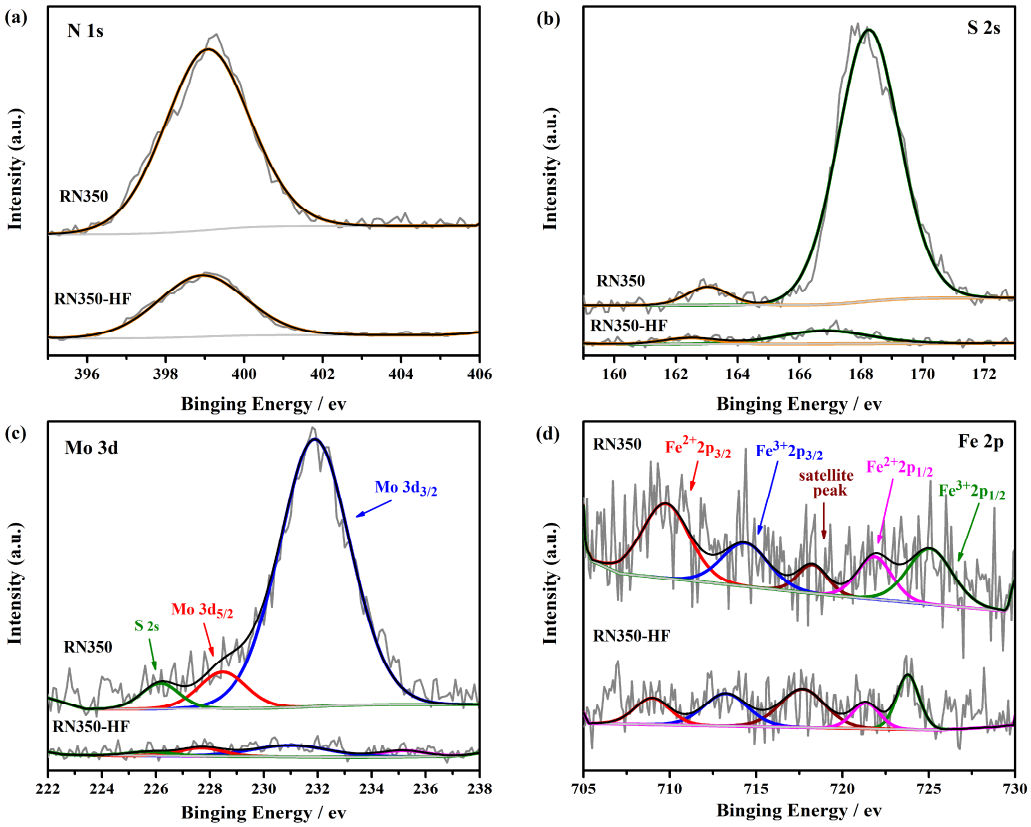

Fig. S9 (a) High-resolution N 1s spectra of RN350 and RN350-HF. (b) High-resolution S 2s spectra. (c) High-resolution Mo 3d spectra. (d) High-resolution Fe 2p spectra.

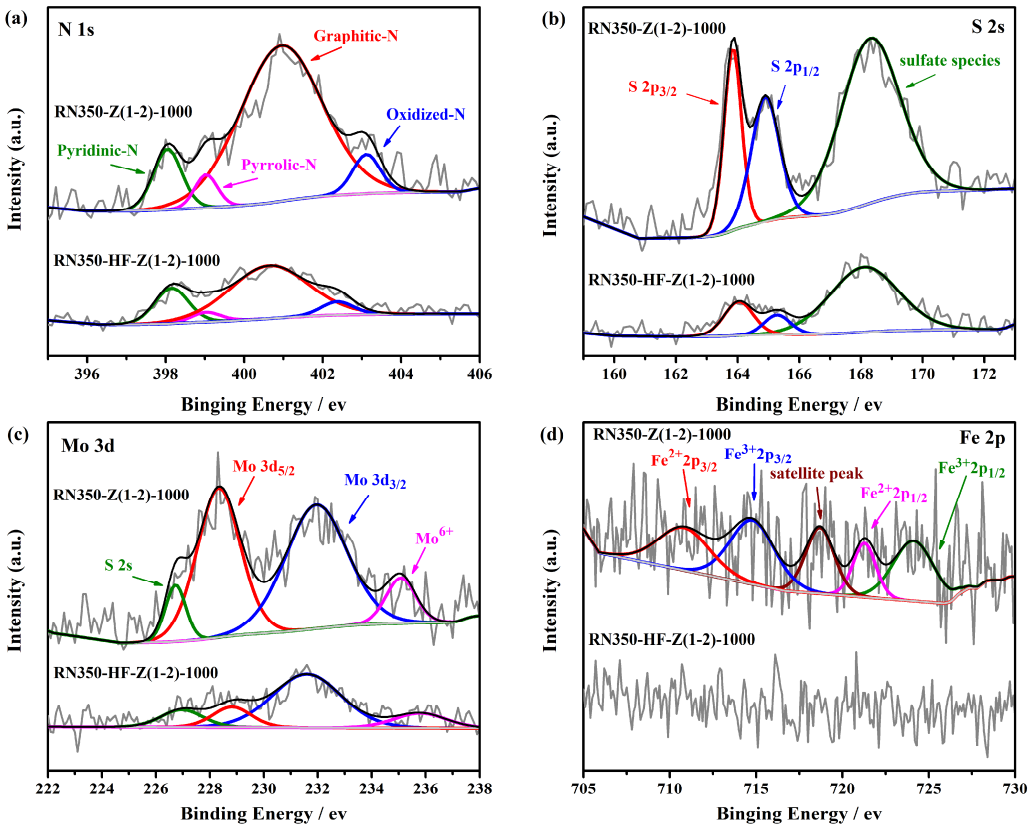

Fig. S10 (a) High-resolution N 1s spectra of RN350-Z(1-2)-1000 and RN350-HF-Z(1-2)-1000. (b) High-resolution S 2s spectra. (c) High-resolution Mo 3d spectra. (d) High-resolution Fe 2p spectra.

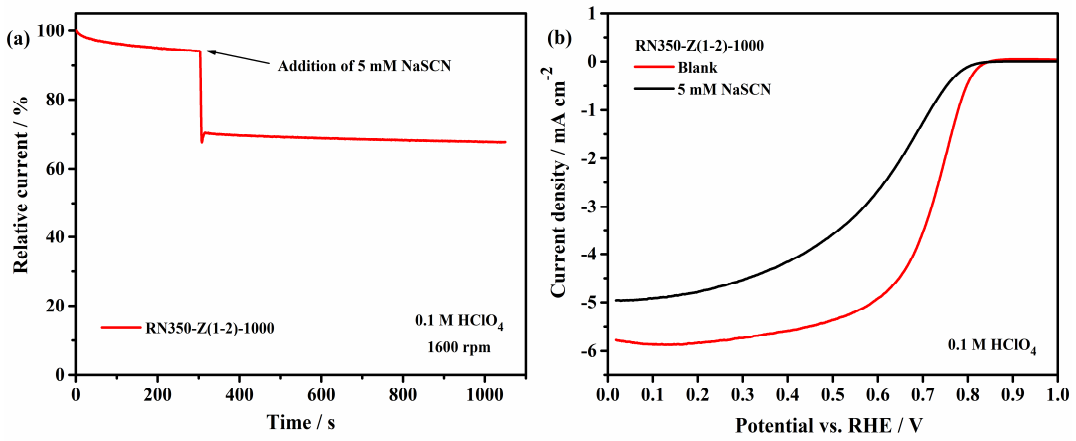

Fig. S11 (a) Current-time curves of the RN350-Z(1-2)-1000 in O_2-saturated 0.1 M $HClO_4$ solution at 0.6 V while 5 mM NaSCN was added at 300 s; (b) LSV curves of electrocatalyst RN350-Z(1-2)-1000 with and without 5 mM NaSCN.

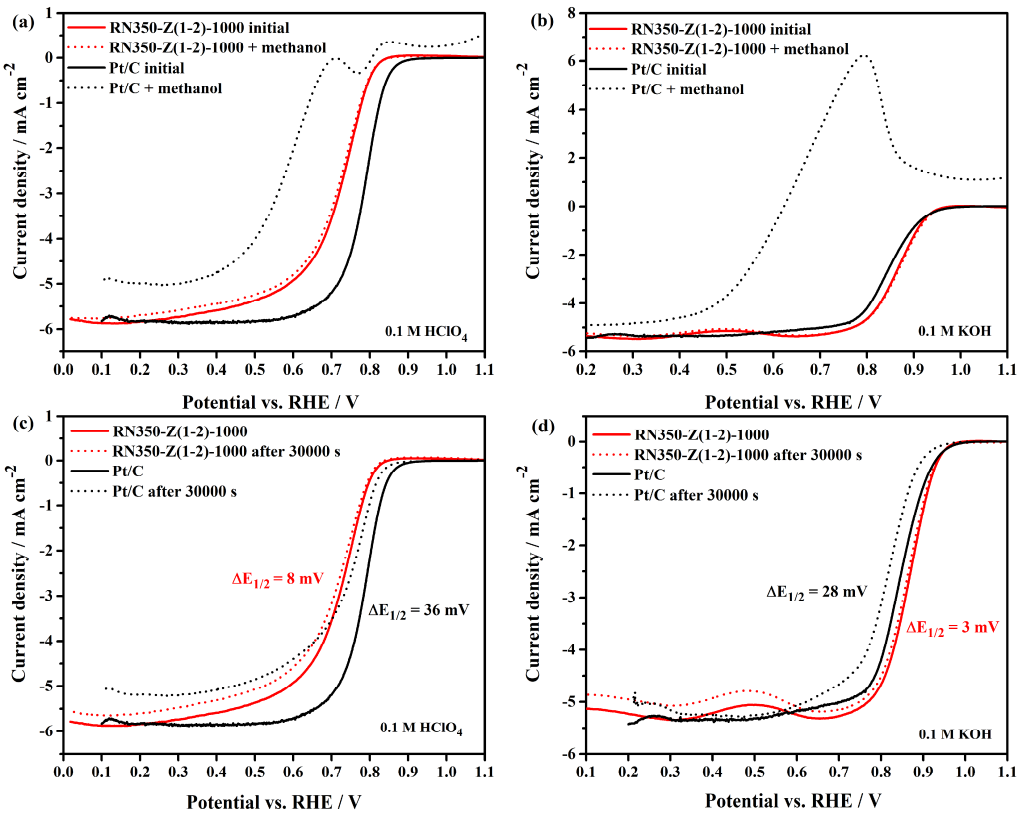

Fig. S12 (a) LSV curves of RN350-Z(1-2)-1000 and Pt/C in O_2-saturated 0.1 M $HClO_4$ solution at a rotating rate of 1600 rpm with/without 1 M methanol. (b) LSV curves of RN350-Z(1-2)-1000 and Pt/C in O_2-saturated 0.1 M KOH solution with/without 1 M methanol. (c) LSV curves of RN350-Z(1-2)-1000 and Pt/C before and after 30000 s durability measurement in O_2-saturated 0.1 M $HClO_4$ solution. (d) LSV curves of RN350-Z(1-2)-1000 and Pt/C before and after 30000 s durability measurement in O_2-saturated 0.1 M KOH solution.

Table S7. The detailed biomass resources and synthesis conditions of each electrocatalysts. The heating rate of all samples is 5 ℃ min^{-1}, and keep at maximum temperature for 2 hours.

Sample	Resource	Precursor	$ZnCl_2$	Mass ratio of Precursor/$ZnCl_2$	Heating Temperature (℃)
RN350	Root nodules	-	-	-	350
RN350-1000	Root nodules	RN350	-	-	1000
RN350-Z(1-2)-700	Root nodules	RN350 (450 mg)	900 mg	1:2	700
RN350-Z(1-2)-800	Root nodules	RN350 (450 mg)	900 mg	1:2	800
RN350-Z(1-2)-900	Root nodules	RN350 (450 mg)	900 mg	1:2	900
RN350-Z(1-2)-1000	Root nodules	RN350 (450 mg)	900 mg	1:2	1000
RN350-Z(1-1)-1000	Root nodules	RN350 (450 mg)	450 mg	1:1	1000
RN350-Z(1-3)-1000	Root nodules	RN350 (450 mg)	1350 mg	1:3	1000
R350	Root	-	-	-	350
R350-Z(1-2)-1000	Root	R350 (450 mg)	900 mg	1:2	1000
S350	Stem	-	-	-	350
S350-Z(1-2)-1000	Stem	S350 (450 mg)	900 mg	1:2	1000
B350	Beans	-	-	-	350
B350-Z(1-2)-1000	Beans	B350 (450 mg)	900 mg	1:2	1000
RN350-HF	Root nodules	RN350	-	-	-
RN350-HF-Z(1-2)-1000	Root nodules	RN350-HF (450 mg)	900 mg	1:2	1000

Table S8. Comparison of biomass sources, synthesis strategies, BET area and ORR performance from this work and recent research reported biomass-derived ORR electrocatalysts in acidic and alkaline medium.

Biomass source	**Heteroatom precursors**	**Other precursors**	**Synthesis strategy**	**Surface area [m^2 g^{-1}]**	**Electrolyte**	**E_{onset} [V] (1600 rpm)**	**$E_{1/2}$ [V]**	**J_L [mA cm^{-2}]**	**Reference**
Legume root nodules	Self-doping (N、S)	$ZnCl_2$, self-doping (Fe、Mo)	Precarbonization, activation, pyrolysis in Ar	1835	0.1 M $HClO_4$	0.827	0.723	5.78	This work
					0.1 M KOH	0.970	0.868	5.23	
Commercial Pt/C (20 %)					0.1 M $HClO_4$	0.882	0.785	5.83	This work
					0.1 M KOH	0.963	0.843	5.34	
Enoki Mushroom	Self-doping (N)	Carbon nanotubes	Ball-milling, pyrolysis in N_2	305.3	0.1 M $HClO_4$	0.81	0.60	2.85	S[1]
					0.1 M KOH	0.94	0.81	3.98	
Cellulose	2-methylimidazole (N)	Co $(NO_3)_2$	MOF growth, Freeze drying, pyrolysis in N_2	235.7	0.5 M H_2SO_4	0.827	0.634	6.45	S[2]
					0.1 M KOH	0.952	0.852	6.4	
Bacterial cellulose	NH_3 (N)	-	Freeze drying, pyrolysis in N_2, second pyrolysis in NH_3	916	0.1 M KOH	-	0.80	5.2	S[3]
Spinach leaves	Self-doping (N、P、S)	$ZnCl_2$	Activation, pyrolysis in Ar	1145	0.1 M KOH	0.95	0.82	5.19	S[4]
Fructus azedarach	H_3PO_4, $NH_4H_2PO_4$ (N、P)	$KHCO_3$	Smash, hydrothermal, activation, pyrolysis in N_2	1584	0.1 M KOH	0.94	0.84	6.01	S[5]
Corn silks	NH_3 (N), Self-doping (P)	$FeCl_3$	Hydrothermal carbonization, pyrolysis in NH_3, doped $FeCl_3$, pyrolysis in NH_3	1038.9	0.1 M KOH	0.957	0.852	5.6	S[6]
Egg	$NH_3{\cdot}H_2O$ (N), self-doping (P)	Si $(OEt)_4$, KOH, self-doping (Fe)	Hydrolysis, spray-dry, carbonization in N_2, silica etching	970	0.1 M KOH	0.84	0.69	4.36	S[7]
Chicken feathers	NH_3 (N) Self-doping (S)	KOH	Precarbonized KOH activation, Pyrolysis in N_2 +NH_3	1098	0.1 M KOH	0.948	0.835	5.33	S[8]

Chicken manure	Hydrazine (N), H_3PO_4 (P)	KOH	Carbonized in Ar, KOH activation, Pyrolysis in Ar, mixing H_3PO_4, pyrolysis, activated in hydrazine	512.2	0.1 M KOH	0.86	0.80	3.94	S[9]
Cystine	NH_3 (N), Self-doping (S)	KOH	Precarbonization, Pyrolysis in Ar, acid washing, pyrolysis in NH_3	1309	0.1 M $HClO_4$	0.809	0.609	6.0	S[10]
					0.1 M KOH	0.953	0.849	5.7	
Coconut palm leaves	Melamine (N)	KOH, $KHCO_3$	Carbonization, activation, pyrolysis in N_2	1419.08	0.5 M H_2SO_4	0.84	0.66	4.97	S[11]
					0.1 M KOH	1.01	0.87	5.5	
Typha orientalis	NH_3 (N)	-	Hydrothermal process, freeze drying, pyrolysis in NH_3	646	0.5 M H_2SO_4	0.725	-	3.3	S[12]
Bamboo stems	Thiourea (N, S)	-	Carbonization, steam activated, mixed with thiourea, pyrolysis in Ar	349.1	0.1 M KOH	-	0.85	4.14	S[13]
Kelps	Self-doping (N, S, P)	$Co(NO_3)_2{\cdot}6H_20$	Pyrolysis in N_2	141.7	0.1 M KOH	0.90	0.74	5.5	S[14]
Reed	1, 10-phen (N)	KOH, $Fe(Ac)_2$	Carbonization, activation, pyrolysis in Ar	534.9	0.1 M KOH	1.00	0.88	5.2	S[15]
Porphyra	Self-doping (N)	KOH, Hemin (Fe)	Activation, carbonization, absorption, pyrolysis in Ar	1499.1	0.1 M KOH	-	0.87	5.0	S[16]
Water hyacinth	Self-doping (N)	$ZnCl_2$	Activation, Pyrolysis in N_2	950.6	0.1 M KOH	0.98	-	4.15	S[17]
Willow catkins	NH_3 (N)	Cobalt (II) acetylacetonate	Pyrolysis, doped Co, pyrolysis in Ar-NH_3	470.1	0.1 M KOH	0.906	0.778	4.5	S[18]
Soybean milk	Self-doping (N)	$FeCl_3$	freeze drying, pyrolysis in N_2	1247	0.1 M NaOH	0.91	0.821	4.5	S[19]
Chlorella	Melamine (N)	$Co(Ac)_2$	Pyrolysis in Ar	728	0.1 M KOH	-	0.87	5.0	S[20]
Chitosan	NH_4Cl (N)	-	freeze drying, pyrolysis in Ar	1005	0.1 M KOH	1.017	0.861	5.2	S[21]

Chitosan	Self-doping (N)	$Zn(NO_3)_2$	Pyrolysis in N_2	794.7	0.1 M KOH	0.96	0.86	6.7	S[22]
Chitosan	Vitamin B12 (N, Co), NH_4OH (N)	SiO_2, Heme (Fe)	Polymerization, Pyrolysis in N_2, HF etching-off SiO_2	225.2	0.1 M $HClO_4$	-	0.70	5.7	S[23]
					0.1 M KOH	-	0.84	5.5	
Cotton fibers	NH_4Cl (N)	-	Pyrolysis in N_2	912.1	0.1 M KOH	0.981	0.82	5.286	S[24]
Silk cocoon	Thiourea (N)	KOH	Pyrolysis in N_2	377	0.1 M KOH	0.853	0.717	4.5	S[25]
cocoon	Self-doping (N, S)	Na_2CO_3, $CaCl_2$, $FeCl_3$	Washing with Na_2CO_3 solution, washing with $CaCl_2$ solution, mixing with $FeCl_3$, freeze-drying, pyrolysis in N_2	714.4	0.1 M KOH	0.94	0.79	3.8	S[26]
Glucose	Thiourea (N, S)	$Co(NO_3)_2$	Polymerization, impregnation, pyrolysis in N_2	667	0.1 M KOH	0.946	0.821	5.5	S[27]
Seaweed	Carbon nanotubes, NH_3 (N)	$CoCl_2$, $NiCl_2$	Freeze-drying, Pyrolysis in NH_3	193	0.1 M KOH	0.89	0.74	4.9	S[28]
Lignin	HNO_3, H_2SO_4, nitration (N)	KCl, $ZnCl_2$	Extraction, aromatic nitration, Pyrolysis in N_2	1589	0.1 M KOH	-	0.85	4.6	S[29]
Pork hearts	Self-doping (N)	KOH	Freeze drying, carbonization, activation, pyrolysis in Ar	1718.84	0.1 M KOH	0.92	0.80	-	S[30]
Cattle bone	Vitamin B12 (N, Co)	KOH	Precarbonization, activation, pyrolysis in Ar, impregnation, pyrolysis in Ar	2520	0.1 M KOH	-	0.835	5.2	S[31]
Cattle bone	Phytic acid (P) Dicyandiamide (N)	KOH	Precarbonization, activation, pyrolysis in Ar, mixing with PA and DCDA, pyrolysis in Ar	1516	0.1 M KOH	-	0.853	-	S[32]

Walnut shells	NH_3 (N)	$FeCl_3$	Pyrolysis in NH_3	714.06	0.1 M KOH	0.847	0.773	5.987	S[33]
Peanut shells	Self-doping (N)	Co $(OH)_2$ (Co) NaH_2PO_2 (P)	Pyrolysis in N_2, activated in CO_2	671.4	0.5 M H_2SO_4	0.89	0.68	3.26	S[34]
					0.1 M KOH	0.91	0.81	5.7	
Keratin	Self-doping (S) NH_3 (N)	KOH	Precarbonized, activation, pyrolysis in N_2, acid-washing, pyrolysis in N_2 +NH_3	1799	0.1 M KOH	0.971	0.842	-	S[35]
Tea leaf residual	Self-doping (N, F)	-	Pyrolysis in N_2	855.6	0.1 M KOH	0.81	0.66	5.1	S[36]

References

1. C. Guo, W. Liao, Z. Li, L. Sun and C. Chen, *Nanoscale*, 2015, **7**, 15990-15998.
2. H. Meng, Y. Liu, H. Liu, S. Pei, X. Yuan, H. Li and Y. Zhang, *ACS Appl. Mater. Interfaces*, 2020, **12**, 41580-41589.
3. H. W. Liang, Z. Y. Wu, L. F. Chen, C. Li and S. H. Yu, *Nano Energy*, 2015, **11**, 366-376.
4. N. B. Huang, J. J. Zhang, Y. Sun, X. N. Sun, Z. Y. Qiu and X. W. Ge, *New J. Chem.*, 2020, **44**, 14604-14614.
5. L. Han, X. Y. Cui, Y. Y. Liu, G. S. Han, X. L. Wu, C. B. Xu and B. J. Li, *Sustain. Energy Fuels*, 2020, **4**, 2707-2717.
6. W. Wan, Q. Wang, L. Zhang, H.-W. Liang, P. Chen and S.-H. Yu, *J. Mater. Chem. A*, 2016, **4**, 8602-8609.
7. H. Wu, J. Geng, H. T. Ge, Z. Y. Guo, Y. G. Wang and G. F. Zheng, *Adv. Energy Mater.*, 2016, **6**.
8. J. Zhu, W. Li, S. Li, J. Zhang, H. Zhou, C. Zhang, J. Zhang and S. Mu, *Small*, 2018, **14**, e1800563.
9. I. L. Alonso-Lemus, M. Z. Figueroa-Torres, D. Lardizabal-Gutíerrez, P. Bartolo-Pérez, J. C. Carrillo-Rodríguez and F. J. Rodríguez-Varela, *Sustain. Energy Fuels*, 2019, **3**, 1307-1316.
10. J. Zhang, H. Zhou, J. Zhu, P. Hu, C. Hang, J. Yang, T. Peng, S. Mu and Y. Huang, *ACS Appl. Mater. Interfaces*, 2017, **9**, 24545-24554.
11. H. Wang, W. Zhang, P. Bai and L. Xu, *Ultrason. Sonochem.*, 2020, **65**, 105048.
12. P. Chen, L. K. Wang, G. Wang, M. R. Gao, J. Ge, W. J. Yuan, Y. H. Shen, A. J. Xie and S. H. Yu, *Energy Environ. Sci.*, 2014, **7**, 4095-4103.
13. M.-J. Kim, J. E. Park, S. Kim, M. S. Lim, A. Jin, O.-H. Kim, M. J. Kim, K.-S. Lee, J. Kim, S.-S. Kim, Y.-H. Cho and Y.-E. Sung, *ACS Catal.*, 2019, **9**, 3389-3398.
14. D. Wu, C. Zhu, Y. Shi, H. Jing, J. Hu, X. Song, D. Si, S. Liang and C. Hao, *ACS Sustain. Chem. Eng.*, 2018, **7**, 1137-1145.
15. Q. L. Wei, X. H. Yang, G. X. Zhang, D. N. Wang, L. Zuin, D. Banham, L. J. Yang, S. Y. Ye, Y. L. Wang, M. Mohamedi and S. H. Sun, *Appl. Catal. B Environ.*, 2018, **237**, 85-93.
16. Z. Zhang, X. Gao, M. Dou, J. Ji and F. Wang, *Small*, 2017, **13**.
17. X. Liu, Y. Zhou, W. Zhou, L. Li, S. Huang and S. Chen, *Nanoscale*, 2015, **7**, 6136-6142.
18. B. Wang, L. Xu, G. P. Liu, P. F. Zhang, W. S. Zhu, J. X. Xia and H. M. Li, *J. Mater. Chem. A*, 2017, **5**,

20170-20179.

19. Y. Y. Liu, J. M. Ruan, S. B. Sang, Z. C. Zhou and Q. M. Wu, *Electrochim. Acta*, 2016, **215**, 388-397.
20. G. Wang, Y. Deng, J. Yu, L. Zheng, L. Du, H. Song and S. Liao, *ACS Appl. Mater. Interfaces*, 2017, **9**, 32168-32178.
21. Y. Wang, J. Hao, J. Yu, H. Yu, K. Wang, X. Yang, J. Li and W. Li, *J. Energy Chem.*, 2020, **45**, 119-125.
22. L. B. Hu, F. Yu, F. Wang, S. C. Yang, B. H. Peng, L. Chen, G. Wang, J. Hou, B. Dai and Z. Q. Tian, *Chin. Chem. Lett.*, 2020, **31**, 1207-1212.
23. Z. Ma, L. Xu, L. Liu, L. Wang, X. Zhang and A. Kong, *Dalton Trans*, 2019, **48**, 2338-2344.
24. X. X. Lin, X. F. Wang, L. G. Li, M. F. Yan and Y. Tian, *ACS Sustain. Chem. Eng.*, 2017, **5**, 9709-9717.
25. Y. X. Wang, Y. P. Lei and H. P. Wang, *Rsc Adv*, 2016, **6**, 73560-73565.
26. C. Q. Li, F. Z. Sun and Y. Q. Lin, *J. Power Sources*, 2018, **384**, 48-57.
27. L. L. Chen, X. P. Guo and G. A. Zhang, *J. Power Sources*, 2017, **360**, 106-113.
28. N. Ma, Y. Jia, X. F. Yang, X. L. She, L. Z. Zhang, Z. Peng, X. D. Yao and D. J. Yang, *J. Mater. Chem. A*, 2016, **4**, 6376-6384.
29. M. Graglia, J. Pampel, T. Hantke, T. P. Fellinger and D. Esposito, *ACS Nano*, 2016, **10**, 4364-4371.
30. B. Yang, J. Gao, M. Xie, S. Zuo, H. Kang, Y. Sun, X. Xu, W. Wang, C. Gao, Y. Liu and J. Yan, *J. Colloid Interface Sci.*, 2020, **579**, 832-841.
31. M. Dou, D. He, W. Shao, H. Liu, F. Wang and L. Dai, *Chemistry (Easton)*, 2016, **22**, 2896-2901.
32. Y. X. Zan, Z. P. Zhang, H. J. Liu, M. L. Dou and F. Wang, *J. Mater. Chem. A*, 2017, **5**, 24329-24334.
33. N. Xue, J. Liu, P. Wang, C. Wang, S. Li, H. Zhu and J. Yin, *J. Colloid Interface Sci.*, 2020, **580**, 460-469.
34. Y. L. Wu, Y. L. Chen, H. Q. Wang, C. M. Wang, A. S. Wang, S. Zhao, X. Y. Li, D. F. Sun and J. Z. Jiang, *J. Mater. Chem. A*, 2018, **6**, 12018-12028.
35. J. Zhang, H. Zhou, X. B. Liu, J. Zhang, T. Peng, J. L. Yang, Y. H. Huang and S. C. Mu, *J. Mater. Chem. A*, 2016, **4**, 15870-15879.
36. D. Y. Wu, Y. T. Shi, H. Y. Jing, X. Wang, X. D. Song, D. H. Si, S. X. Liang and C. Hao, *Int. J. Hydrogen Energy*, 2018, **43**, 19492-19499.